ACS APPLIED MATERIALS & INTERFACES

Research Article

www.acsami.org

Large-Area, Conductive and Flexible Reduced Graphene Oxide (RGO) Membrane Fabricated by Electrophoretic Deposition (EPD)

Mei Wang,[†] Le Dai Duong,[†] Joon-Suk Oh,[‡] Nguyen Thi Mai,[†] Sanghoon Kim,[†] Seungchul Hong,[‡] Taeseon Hwang,[‡] Youngkwan Lee,[§] and Jae-Do Nam*[,†,‡]

[†]Department of Energy Science, Sungkyunkwan University, Suwon, 440-746, South Korea

[‡]Department of Polymer Science and Engineering, Sungkyunkwan University, Suwon, 440-746, South Korea

[§]Department of Chemical Engineering, Sungkyunkwan University, Suwon, 440-746, South Korea

Supporting Information

ABSTRACT: A large-area, conductive, and flexible membrane made from the stabilized aqueous solution of reduced graphene oxide (RGO) is successfully fabricated using an electrophoretic deposition (EPD) method. A low-voltage operation of EPD (~3 volts) allows a robust consolidation of RGO layers desirably aligned in the in-plane direction through the cohesive electrophoretic squeezing force near the current collector. Transferring the deposited RGO layers to arbitrary substrates or achieving as a free-standing form, two methods of "chemical etching" and "electrochemical etching" are developed to detach the RGO layers from the EPD current collector without damaging the deposited RGO. Further reducing the free-standing RGO membrane by thermal annealing up to 1000 °C, a graphite-like architecture is restored (*d*-spacing at 3.42 Å with C/O ratio at 16.66) and the electrical conductivity increases as high as 5.51×10^5 S/m. The tightly-consolidated and securely-detached RGO membrane allows the free-standing and flexible features and highly conductive characteristics, which are further developed during thermal treatment. Because of the facile scale-up nature of the EPD process and RGO solution, the developed methodology has a considerable potential to be applied to various energy storage devices, flexible conductive coatings, and other electrochemical systems.

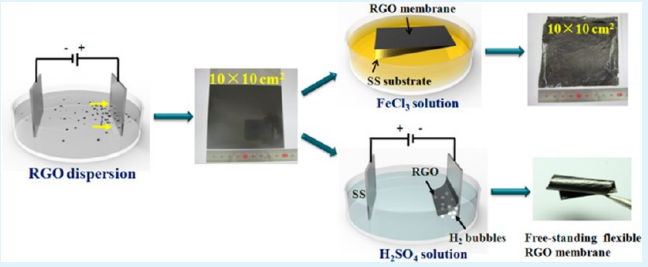

KEYWORDS: *RGO membrane, EPD, free-standing, large-area, flexible, conductive*

INTRODUCTION

Graphene membranes have attracted significant attention because of their excellent electronic, mechanical, and thermal properties, making them applicable for conducting transparent electrodes,[1] electrical batteries,[2] supercapacitors,[3] fuel cells,[4] protective layers,[5,6] transistors,[7,8] field-emitters,[9] and sensors.[10] For the full-scale application of graphene in these fields, a scalable production method of large-area graphene films is required.[11] Hence, there is a need to develop a fabrication technique with scalable and high-throughput capacity. Various graphene membrane preparation methods have been proposed, such as membrane filtration,[12] electrophoretic deposition (EPD),[13] chemical vapor deposition (CVD),[1] spin coating,[14] layer-by-layer (LBL) electrostatic self-assembly,[15] and spray coating.[16] Recently, the reduced graphene oxide (RGO) binder-free free-standing membrane is prepared from a stabilized aqueous RGO solution using a membrane filtration method,[17] but the size and shape of the RGO membrane is limited with this method. In the case of LBL self-assembly[18] and CVD methods,[19,20] it is practically difficult to obtain thick graphene membranes (>600 nm). In addition, it should be mentioned that the self-assemble method usually needs surfactants.[15] The graphene membrane prepared using the spin coating or spray coating method is usually restricted by the size and uniformity of the membrane, as well as bad packing morphology especially when a thick graphene membrane is to be fabricated.

EPD provides the possibility of scaling up the area of the RGO membrane, as well as obtaining good membrane morphology and uniformity. EPD is a nanoscale assembly process that colloidal particles suspended in a liquid medium migrate under an electric field and deposit onto the electrode; it therefore offers the advantages of high deposition/production rates, wide-range thickness adjustment, low cost, uniformity of deposits, etc. EPD provides the scalability of deposits, as demonstrated by applications in the ceramics and coatings industries, where the size of deposited films vary from as large as automotive bodies to as small as nanoscale electrodes.[21] Thus, the large-scale manufacturing of RGO membrane by EPD method can be easily achieved by using large-area electrode (e.g., plate and roll-to-roll electrode).[22]

Received: October 25, 2013
Accepted: January 16, 2014
Published: January 16, 2014

   dx.doi.org/10.1021/am404719u | *ACS Appl. Mater. Interfaces* 2014, 6, 1747−1753

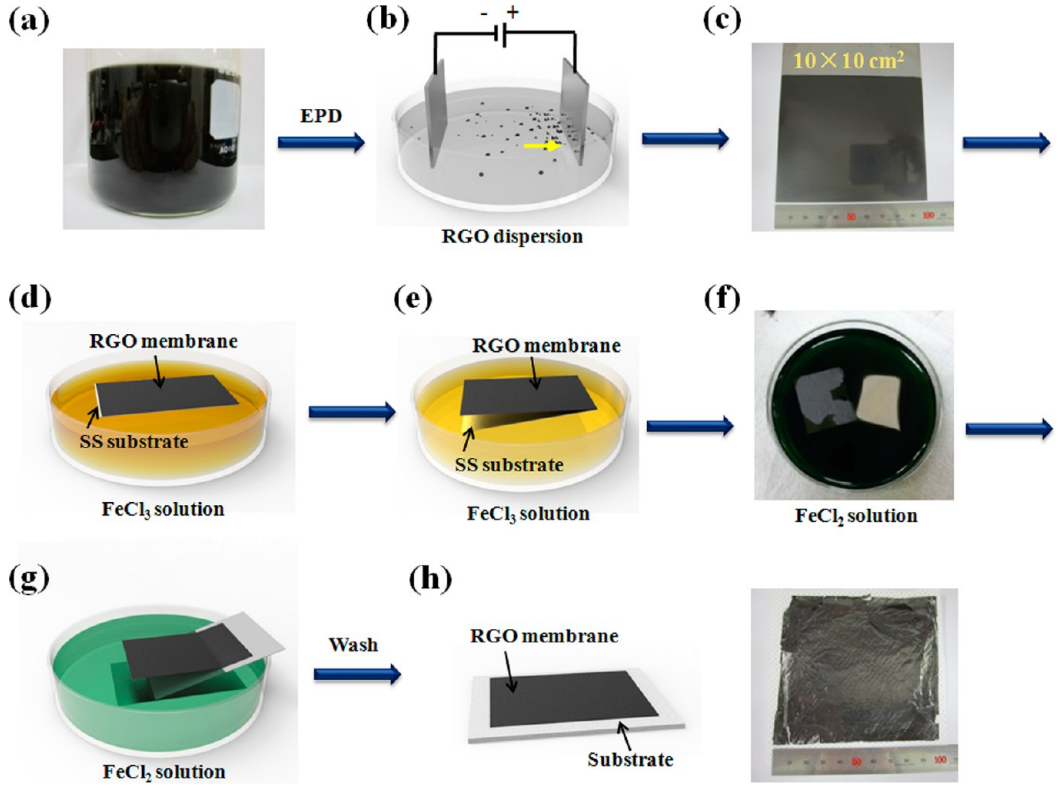

Figure 1. Schematic representation of the preparation and detaching process of RGO membrane. (a) Homogeneous aqueous solution of RGO. (b) EPD process of RGO. (c) RGO membrane deposited on the SS with the size of 10×10 cm^2. (d) RGO/SS plate floating on the $FeCl_3$ solution surface. (e) Detachment of the RGO membrane from SS. (f) RGO membrane separated from the SS floating on the solution surface. (g) Scooping of the RGO membrane by the target substrate. (h) RGO transferred to any substrate (left) or obtained as a free-standing membrane (right) with the size of 10 × 10 cm^2.

In the EPD of RGO from aqueous suspensions, the uncontrollable agglomeration of RGO in aqueous solution usually hampers the successful fabrication of RGO membranes. Various techniques have been reported to produce graphene or RGO by chemical reduction from graphene oxide (GO), such as chemical reduction,[23] electrochemical reduction,[24,25] thermal reduction,[14] and vapor-phased reduction.[26] Among these techniques, the chemical reduction by hydrazine or dimethylhydrazine has been most commonly used because of its good compatibility with water, which often facilitates the preparation of a stable RGO aqueous solution. Recently, we successfully develop a low-temperature reduction approach ensuring the large-scale production of a stable aqueous RGO solution without using any surfactant stabilizers and organic solvents,[17] which subsequently allow the EPD method for the production of large-area RGO membranes. To fully restore the conductivity of RGO membrane, the thermal annealing is usually utilized as a subsequent deoxygenation process.[27,28] By removing the oxygen-containing groups under high temperature, the RGO is highly reduced, and thus, the conductivity of RGO membrane can be increased.

RGO membranes have been reported to be prepared by EPD method, for the applications including supercapacitors, solar cells, field emission devices and transparent conductors.[29,30] While, the method to detach the RGO membrane from substrate has not been reported in these literatures, limiting the full-scale application of RGO membrane such as flexible and free-standing RGO membrane and RGO coated on a nonconductive substrate. Therefore, a facile detaching method with high efficiency is needed, which enable the RGO membrane to be free-standing or transferable. We may detach the RGO film from the substrate by sacrificing the substrate or breaking the interfacial bonding between the RGO and the substrate.[1,31] The RGO films detached from the EPD substrate may be transferred to other substrates such as a glass slide, silicon wafer, polyethylene terephthalate (PET) film, metal foil, etc.

Herein, we develop an efficient method to fabricate large-area RGO membranes using EPD. We also describe two detaching methods of RGO membrane from the EPD substrate via chemical etching or electrochemical etching. Using these methods, the RGO film stacked by EPD is transferred to other substrates or achieved as a free-standing membrane. Furthermore, we demonstrate that the excellent packing morphology and high sheet conductivity are obtained after further thermal annealing of the large-area RGO membrane.

EXPERIMENTAL SECTION

Material Preparation. Graphite oxide was oxidized from graphite (Sigma-Aldrich) using the modified Hummers method. Graphite oxide (0.6 g) was exfoliated in 400 mL of DI water with ultrasonication for 4 h, followed by centrifugation at 4000 rpm for 15 min, to obtain a homogeneous GO solution. The aqueous RGO solution was prepared using the rate-controlled reduction method, as we previously reported.[17] The GO suspension was cooled down to 0-5 °C in the ice bath, followed by the dropwise addition of 5 mM hydrazine solution (35 wt %, Sigma-Aldrich). Subsequently, further reduction was carried out by heating the RGO suspension on a flat heater at 200 °C for 30 min. The suspension was mildly stirred with a magnetic bar throughout the reduction process. The electrophoretic deposition of RGO was carried out directly in the aqueous suspension at room temperature. A direct current (DC) voltage of 3 V was applied to the

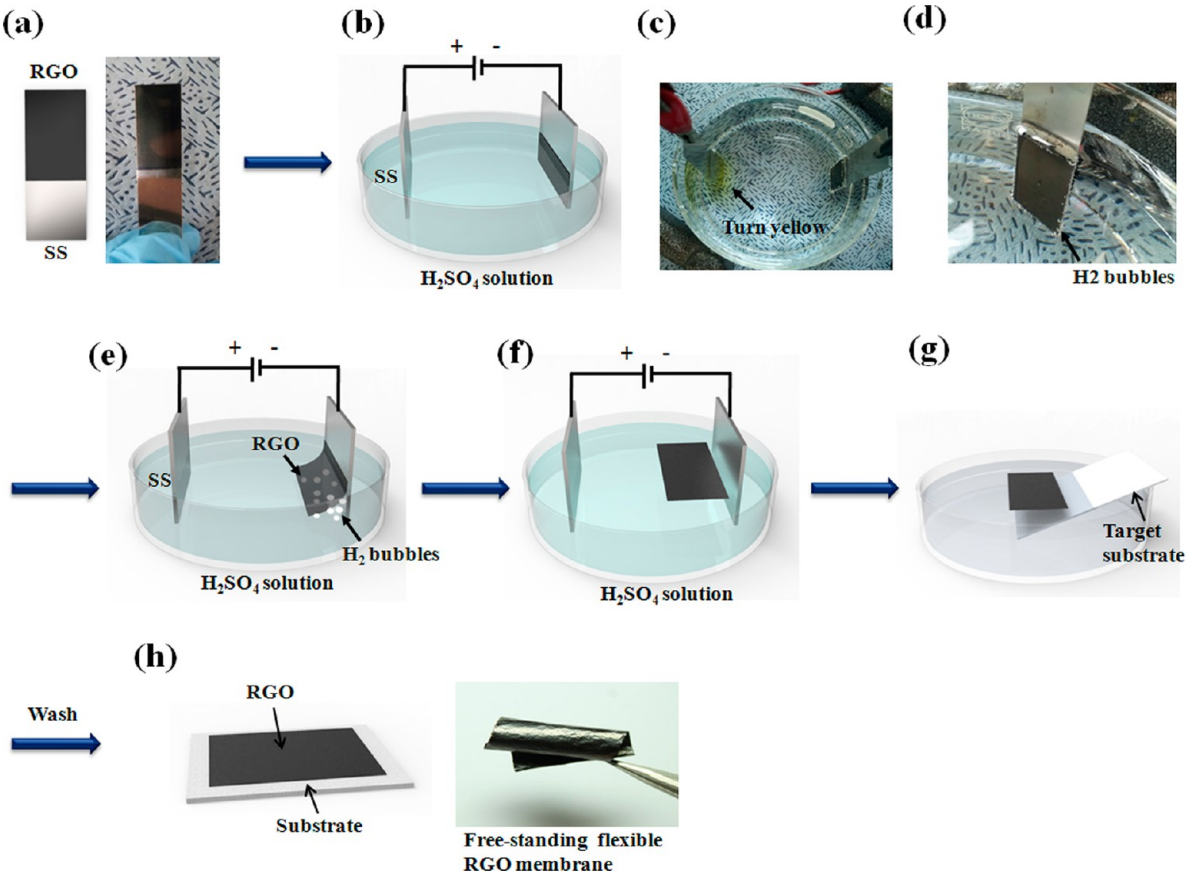

Figure 2. Schematic representation of the preparation and detaching process of RGO membrane by EPD. (a) RGO membrane deposited on SS substrate by EPD. (b) Direct voltage is applied to the RGO/SS cathode and an SS anode in the electrolyte of the H_2SO_4 solution. (c) Digital image of the electrolytic cell. (d) Digital image of the RGO/SS cathode, where bubbles start to emerge on the edge of electrode. (e) RGO membrane starts to detach from the SS with the assistance of H_2 bubbles. (f) RGO membrane detaches from the SS and floats on the surface of the solution. (g) Scooping of the RGO by target substrate. (h) The RGO can be transferred to an arbitrary substrate (left) or can be a free-standing membrane (right).

stainless steel (SS) electrodes for 15 min and RGO was deposited on the anode electrode. During the entire reduction and EPD process, the suspension was mildly stirred with a magnetic bar. After EPD deposition, samples were washed with deionized (DI) water and dried in air at room temperature.

The prepared RGO membrane deposited on the SS was detached by etching the stainless substrate with $FeCl_3$ solution (25 wt %, Sigma-Aldrich). The RGO/SS plate was placed on the surface of the $FeCl_3$ solution surface (with the RGO side facing up). After the RGO/SS interface was etched, the SS plate sank under the water and the RGO membrane floated to the solution surface. The RGO film on the solution surface was then transferred by scooping up the RGO film using polypropylene paper (Kimtech). The RGO was washed by repeatedly transferring the RGO film to the surface of the DI water and subsequently scooping it out using a polypropylene wiper. After it was washed, the RGO membrane was dried at room temperature. The RGO membrane can then be easily detached from the wiper.

In the electrochemical etching process, the direct voltage of 5 V was applied to the RGO/SS cathode and the SS anode in the electrolyte of the 0.6 M H_2SO_4 solution. Hydrogen bubbles emerged at the RGO/SS interfaces, providing forces to detach the RGO membrane from the SS. After peeling off from SS plate, the RGO film could be scooped up by the wiper. For the delamination of a thin RGO membrane (<500 nm), a poly methyl methacrylate (PMMA) layer needed to be spin-coated on the RGO as a protective layer; after being detached from the substrate, the PMMA could be washed out with acetone.

The free-standing RGO membrane was further annealed at a high temperature. The RGO membrane was packed between two stacked quartz plates and then transferred to the chamber of a temperature-programmed furnace. Argon gas was pumped into the chamber at a flow rate of 10 sccm. The thermal treatment of the RGO membrane was performed at 200, 400, 600, 800, and 1000 °C for 5 h.

Characterization. The microstructure of the RGO membranes was characterized by field emission scanning electron microscopy (FE-SEM, JEOL, JEM 7000F, Japan). The interlayer information of samples was obtained by X-ray diffractometry (XRD, Rigaku Rotaflex D/Max) with a Cu Kα radiation (λ = 0.154 nm) in the 2θ range from 5 to 40 degrees with a scanning speed of 4°/min. Raman spectroscopy (WITec, alpha 300 M) with a wavelength of 532 nm was used. The sheet resistance of all samples was measured using a four-point probe method (Keithley) at room temperature. Thermal gravimetric analysis (TGA, SEICO, Seiko Exstar 6000) was used for structural and composition analysis of RGO. The temperature was increased from 80 to 1000 °C at a ramping rate of 5 °C/min under N_2 atmosphere. X-ray photoelectron spectroscopy (XPS, QUANTUM 2000, Physical electronics, USA) was performed using the focused monochromatized Al Ka radiation ($h\nu$ = 1486.6 eV), which was corrected by the C1s line at 284.6 eV. Sheet resistance and conductivity measurements were performed using a four-point method (Keithley 2420I-V) at room temperature.

RESULTS AND DISCUSSION

Figure 1 shows a schematic representation of the EPD stacking process and "chemical detaching" method for detaching the RGO membrane from the EPD substrate. The EPD process is applied directly in the RGO aqueous suspension (Figure 1a) with the voltage of 3 V (Figure 1b). The RGO membrane with

dx.doi.org/10.1021/am404719u | ACS Appl. Mater. Interfaces 2014, 6, 1747−1753

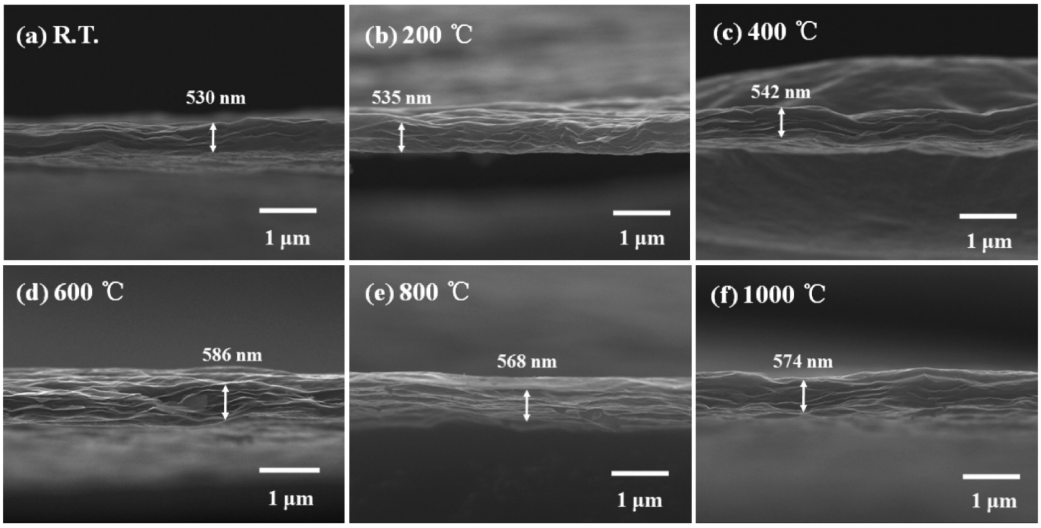

Figure 3. Cross-sectional FE-SEM images of deposited RGO membranes annealed at different temperatures: (a) RT, (b) 200, (c) 400, (d) 600, (e) 800, and (f) 1000 °C. The membranes are detached from SS substrate by electrochemical etching method.

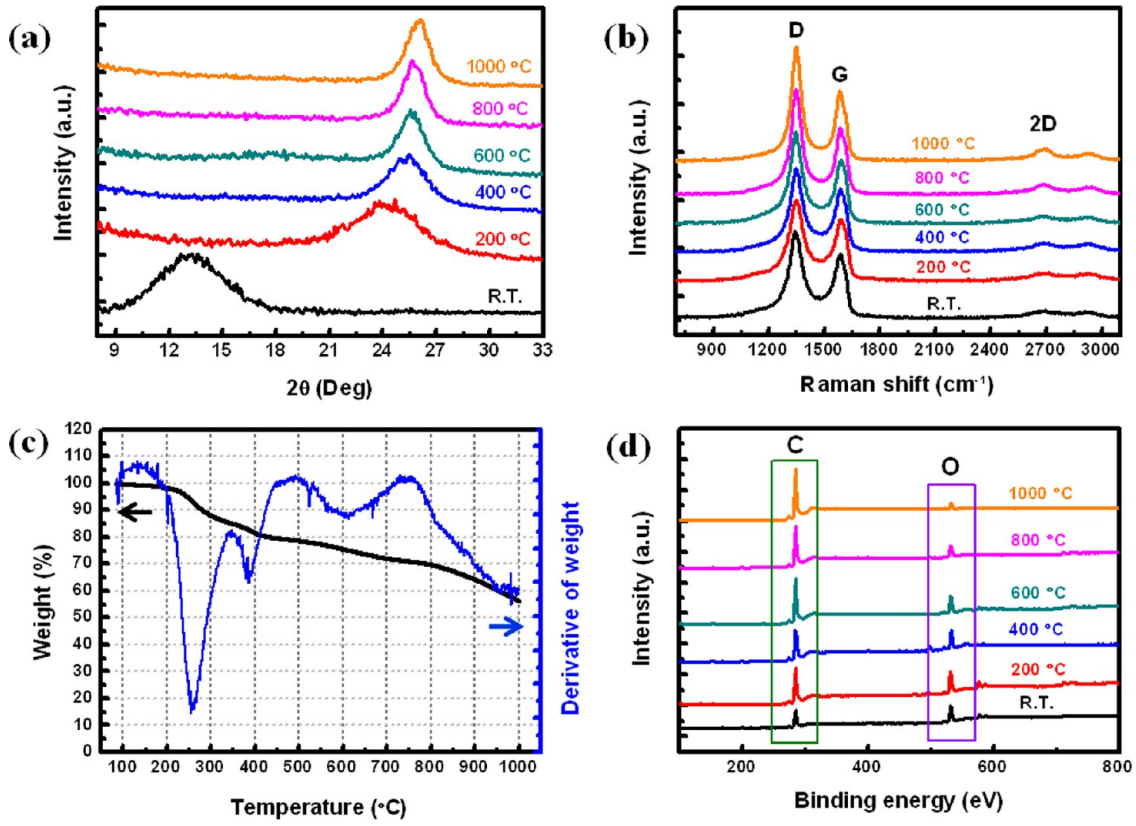

Figure 4. (a) X-ray diffraction (XRD) spectroscopy data of RGO membranes prepared by EPD and subsequent thermal annealing. (b) Raman spectra of RGO membranes at an excitation wavelength of 532 nm. (c) TG and DTG of RGO prepared by EPD. (d) X-ray photoelectron spectroscopy (XPS) wide scan spectra of RGO membranes annealed at different temperatures.

the size of 10 × 10 cm^2 is deposited on the positive electrode because of the negative charges of RGO layers. After the RGO membrane was dried at room temperature (Figure 1c), the surface of the RGO membrane becomes shiny and gray in color with a smooth surface. Subsequently, the RGO membrane on the stainless steel (SS) substrate is placed floating onto the surface of the $FeCl_3$ aqueous solution, as shown in Figure 1d. The interface between the SS and the RGO membrane is etched slowly and finally the RGO membrane and SS are separated (Figure 1e) via reduction of Fe^{3+}, namely, Fe (s) + $2Fe^{3+}$ (aq) → $3Fe^{2+}$ (aq). As the interface is etched, the solution becomes a dark green color as shown in Figure 1f. Figure 1f also shows the camera picture of the detached RGO membrane floating freely on the surface of the $FeCl_2$ solution, which can further be transferred to other substrates. Subsequently, the RGO membrane is transferred onto the target substrate (Figure 1g and 1h). To obtain a free-standing RGO film, a porous polypropylene paper is used in this study

dx.doi.org/10.1021/am404719u | ACS Appl. Mater. Interfaces 2014, 6, 1747−1753

Table 1. Properties of RGO Membranes with Different Annealing Temperatures

sample name	XPS C/O ratio	Raman I_D/I_G	XRD 2θ (deg)	thickness (nm)	sheet resistance (Ω/sq)	conductivity (S/m)
RGO-RT	2.60	1.12	13.16	530	329.16	5.73×10^3
RGO-200	3.67	1.08	24.01	535	105.50	1.77×10^4
RGO-400	4.77	1.09	25.36	542	8.69	2.12×10^5
RGO-600	5.29	1.12	25.61	586	6.20	2.75×10^5
RGO-800	7.49	1.17	25.68	568	3.84	4.58×10^5
RGO-1000	16.66	1.18	26.05	574	3.16	5.51×10^5

to minimize the adhesion to the substrate. After it was washed with H_2O and dried at room temperature, the RGO membrane will automatically detach from the polypropylene paper, resulting in a large-area free-standing membrane (Figure 1h (right)). The chemical etching method can be applied on various metal substrates such as Ni foil/foam, stainless steel foil, Cu foil, and Al foil.

As an alternative, the "electrochemical etching" is schematically shown in Figure 2, where the RGO membrane is stripped from the EPD electrode by water electrolysis. During the electrochemical etching, a direct current of 5 V is applied to the RGO/SS cathode and an SS anode in the electrolyte of the 0.6 M H_2SO_4 solution (Figure 2b-d). Hydrogen bubbles appear at the RGO/SS interfaces (Figure 2e) because of the electrolysis of the H_2SO_4 solution: $2H^+$ (aq) + $2e^-$ → H_2 (g). H_2 bubbles provide a gentle but persistent force to detach the RGO membrane from the SS at its edges, and the process is aided by the permeation of the electrolyte solution into the interlayers as the edges are detached.[32] On the other hand, the dissolution of Fe in SS anode complies with Fe (s) − $3e^-$ → Fe^{3+} (aq). Subsequently, the solution near the anode becomes faint yellow (Figure 2c). After being peeled off from the SS plate and scooped from the solution (Figure 2f and 2g), the RGO film can be obtained as a free-standing form or transferred to any other substrates (Figure 2h and Supporting Information Figure S1). The electrochemical etching method can be widely applied on not only metal substrate, but also other substrate such as ITO/FTO glass and graphite paper. As demonstrated in Figures 1 and 2, both chemical and electrochemical etching methods developed in this study can be easily scaled up to a large-volume and low-cost production.

Figure 3 presents the FE-SEM images of the RGO membrane annealed at different temperatures. As presented in Figure 3a, the surface RGO membrane shows a typical undulating and wrinkled RGO surface morphology.[33] It clearly shows that the RGO layers are tightly stacked in the in-plane direction under the electric field force. Figure 3b−3f shows the cross-sectional images of RGO membranes with annealing temperatures at 200, 400, 600, 800, and 1000 °C, respectively. The RGO membranes are annealed between two quartz plates,[28] the generated gases are then guided to spread in the in-plane direction during the annealing process. Thus, the RGO membranes have no obvious thickness difference in the in-plane direction after thermal treatment under high temperature (Figure 3b−3f), which should be compared with the RGO membrane annealed at 600 °C without quartz squeezing (Supporting Information Figure S2). It is worth noting that, as shown in Figure 3a and Supporting Information Figure S3, the thickness and morphology of RGO membranes detached by electrochemical etching and chemical etching method give no obvious difference, indicating the same effects of two detaching methods.

The X-ray diffraction spectroscopy (XRD) and Raman spectroscopy demonstrate the reduction of RGO during the thermal annealing process. As shown in Figure 4a and Table 1, the characteristic peak of RGO appears at 2θ = 13.24° (d-spacing ≈ 6.68 Å). This 2θ value is larger than the typical 2θ value of GO (∼10°) because the removal of the oxygen-containing functional groups in RGO during the hydrazine reduction process can decrease the interlayer space, resulting in an increase of a 2θ degree value. As the annealing temperature increases to 1000 °C, the 2θ shifts to 26.05° (d-spacing ≈ 3.42 Å) because of the release of oxygen-functional groups under high temperature. Figure 4b shows Raman spectra of RGO membranes prepared using the EPD method at different annealing temperatures. A D-band at 1343 cm^{-1} and a G-band around 1588 cm^{-1} appear in the spectra, similarly to the previous work.[34] The D-band intensity of the as-prepared RGO is relatively high because of the sp^3 hybridization of carbon atoms during the oxidation from graphite.[35] The G-band is attributed to the recovery of the hexagonal network of C atoms with defects. The intensity ratio of the D- and G-bands (I_D/I_G) provides a sensitive measure of the disorder and crystallite size of the graphitic layers.[36] The D-band intensity is higher than that of the G-band, indicating that a high quantity of structural defects and disorder are introduced to the RGO during the oxidation and reduction process. As presented in Table 1, the I_D/I_G of RGO decreases from 1.12 to 1.08 as the annealing temperature increases to 200 °C. From 200 to 1000 °C, the oxygen-functional groups are released as CO and CO_2, inducing more defects in the carbon backbone and causing the I_D/I_G to increase from 1.08 to 1.18.[28] Furthermore, we note a blue shift of G peak position from 1588 (200 °C) to 1584 cm^{-1} (1000 °C) because the removal of oxygen-containing groups reduces the electron withdrawing ability of these groups. In addition, the intensity of the 2D (2686 cm^{-1}) peaks increases in the Raman spectra as the annealing temperature increases, indicating that graphitization in the RGO occurs during the reduction process.[26]

Figure 4c shows the TGA and differential thermogravimetric (DTG) curves of RGO prepared by EPD. Three DTG peaks are observed at 260, 388, and 614 °C. As shown in Figure 4c, a 19.7% weight loss occurs from 200 to 500 °C, corresponding to the decomposition of functional groups such as hydroxyl, carboxyl, and epoxide groups.[37] The small molecules that are released were determined to be H_2O, CO, CO_2, and radical C.[28] The 22.3% smooth weight loss from 500 to 1000 °C and the DTG peak at 614 °C correspond to the further deoxygenation from the sp^2 graphitic lattice. Finally, 43.9% of mass is lost as the temperature reaches 1000 °C.

Furthermore, the C1s spectra of the RGO membranes further demonstrate that the RGO is continuously reduced by the thermal annealing, as shown in Figure 4d. For the RGO prepared by EPD, the peak intensities of carbon and oxygen give relative contents of 72.2% and 27.8%, respectively. The

C1s peaks shown in Supporting Information Figure S4 are reasonably composed of four Gaussian peaks with binding energies of 284.6 (nonoxygenated C ring, C═C/C−C), 286.0 (hydroxyl and epoxy, C−O), 287.3 (carbonyl, C═O), and 288.8 eV (carboxyl, O−C═O).[38] The remaining oxygen-containing functional groups enhance the stability of RGO dispersion in the liquid phase and, subsequently, provide negative charges to the RGO layers, which desirably facilitates the EPD process of RGO sheets. As the annealing temperature increases to 1000 °C, the content of C increases but the content of O decreases, rapidly increasing the C/O ratio to 16.66 (Supporting Information Table S1 and 1). After the annealing of the membranes, the narrow scan spectra of C1s are revealed as shown in Supporting Information Figure S4, which additionally confirms the removal of oxygen from the membrane during annealing. As the annealing temperature increases, it can be seen that the total contents of oxygen functionalities (C−O, C═O, and O−C═O) are obviously decreased.

The sheet resistance and conductivity of RGO membranes are shown in Figure 5 and Table 1, which are evaluated using

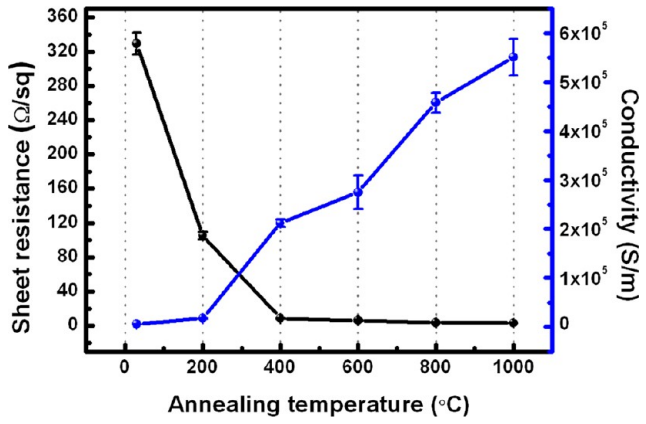

Figure 5. Sheet resistance and conductivity of RGO membranes annealed at different temperatures.

the methods reported in previous literatures.[17,39] As the annealing temperature increases, the sheet resistance clearly decreases along with the rapid increase of conductivity of RGO. The sheet resistances of annealed RGO are decreased due to the elimination of oxygen functionalities and the effective interlaminar consolidation. Notably, the conductivity of our RGO membrane annealed at 1000 °C is more than three times higher than the reported values of the RGO membrane prepared by the vacuum filtration method annealed at 1900 °C.[17] We believe that the excellent conductivity of our RGO membranes stems from the tightly-consolidated layer-by-layer packing and, more importantly, the well-aligned sheet morphology in the in-plane direction.

CONCLUSIONS

In this study, we report a novel method to prepare a free-standing RGO membrane or a RGO membrane coated on arbitrary substrates by EPD. A large-sized flexible RGO membrane of 10 × 10 cm^2 is successfully obtained by our preparation method, which has not previously been reported. Two methods of detaching the RGO membrane from the EPD substrate are also reported. The RGO membrane fabricated in our method shows a smooth surface and tight packing morphology. The uniform layer-by-layer packing structure provides a simple electron conductive route in the in-plane direction, giving an excellent electrical conductivity of the membrane. Thermal annealing is applied on the RGO membrane and the layer-by-layer structure is successfully preserved, notably improving the conductivity of the RGO membranes. The freestanding, flexible and highly conductive RGO membranes have considerable potential for application in electrical devices. Further study and optimization of this process should be carried out in the future.

ASSOCIATED CONTENT

Supporting Information

Additional flexibility test, SEM images, C1s spectra, and C and O atomic composition list of RGO membranes. This material is available free of charge via the Internet at http://pubs.acs.org.

AUTHOR INFORMATION

Corresponding Author

*E-mail: jdnam@skku.edu. Tel.: +82-31-290-7285. Fax: +82-31-292-8790.

Author Contributions

The manuscript was written through contributions of all authors. All authors have given approval to the final version of the manuscript.

Notes

The authors declare no competing financial interest.

ACKNOWLEDGMENTS

This research was supported by the World Class University (WCU) program (R31-2008-10029) and research grants (2010-0028939, 2012-0006672) through the National Research Foundation of Korea funded by the Ministry of Education, Science and Technology. We also appreciate the project and equipment support provided by Gyeonggi Province through the Gyeonggi Regional Research Center (GRRC) at Sungkyunkwan University.

REFERENCES

(1) Kim, K.; Zhao, Y.; Jang, H.; Lee, S.; Kim, J.; Kim, K. S.; Ahn, J.; Kim, P.; Choi, J.; Hong, B. H. *Nature* **2009**, *457*, 706−710.
(2) Reddy, A. L. M.; Srivastava, A.; Gowda, S. R.; Gullapalli, H.; Dubey, M.; Ajayan, P. M. *ACS Nano* **2010**, *4*, 6337−6342.
(3) Lai, L.; Yang, H.; Wang, Liang.; Teh, B. K.; Zhong, J.; Chou, H.; Chen, L.; Chen, W.; Shen, Z.; Ruoff, R. S.; Lin, J. *ACS Nano* **2012**, *6* (7), 5941−5951.
(4) Liu, S.; Wang, J.; Zeng, J.; Ou, J.; Li, Z.; Liu, X.; Yang, S. *J. Power Sources* **2010**, *195*, 4628−4633.
(5) Chen, T. L.; Ghosh, D. S.; Formica, N.; Pruneri, V. *Nanotechnology* **2012**, *23*, 395603.
(6) Prasai, D.; Tuberquia, J. C.; Harl, R. R.; Jennings, G. K.; Bolotin, K. I. *ACS Nano* **2012**, *6*, 1102−1108.
(7) Burghard, M.; Klauk, H.; Kern, K. *Adv. Mater.* **2009**, *21*, 2586−2600.
(8) Liu, W.; Jacson, B. L.; Zhu, J.; Miao, C.; Chung, C.; Park, Y.; Sun, K.; Woo, J.; Xie, Y. *ACS Nano* **2010**, *4*, 3927−3932.
(9) Jiang, L.; Yang, T.; Liu, F.; Dong, J.; Yao, Z.; Shen, C.; Deng, S.; Xu, N.; Liu, Y.; Gao, H. *Adv. Mater.* **2013**, *25*, 250−255.
(10) Allen, M. J.; Tung, V. C.; Kaner, R. B. *Chem. Rev.* **2010**, *110*, 132−145.
(11) Cao, X.; Qi, D.; Yin, S.; Bu, J.; Li, F.; Goh, C. F.; Zhang, S.; Chen, X. *Adv. Mater.* **2013**, *25*, 2957−2962.
(12) Hwang, T.; Oh, J. S.; Hong, J.; Nam, G.; Bae, A.; Son, S.; Lee, G.; Sung, H.; Lee, Y.; Nam, J. *Carbon* **2012**, *50*, 612−621.

(13) An, S. J.; Zhu, Y.; Lee, S. H.; Stoller, M. D.; Emilsson, T.; Park, S.; Velamakanni, A.; An, J.; Ruoff, R. S. *J. Phys. Chem. Lett.* **2010**, *1*, 1259−1263.
(14) Becerril, H. A.; Mao, J.; Liu, Z.; Stoltenberg, R. M.; Bao, Z.; Chen, Y. *ACS Nano* **2008**, *2*, 463−470.
(15) Yu, D.; Dai, L. *J. Phys. Chem. Lett.* **2010**, *1*, 467−470.
(16) Pham, V. H.; Cuong, T. V.; Hur, S. H.; Shin, E. W.; Kim, J. S.; Chung, J. S.; Kim, E. J. *Carbon* **2010**, *48*, 1945−1951.
(17) Ghosh, T.; Biswas, C.; Oh, J.; Arabale, G.; Hwang, T.; Luong, N. D.; Jin, M.; Lee, Y. H.; Nam, J. *Chem. Mater.* **2012**, *24*, 594−599.
(18) Park, J. S.; Cho, S. M.; Kim, W.; Park, J.; Yoo, P. J. *ACS Appl. Mater. Interfaces* **2011**, *3*, 360−368.
(19) Miller, J. R.; Outlaw, R. A.; Holloway, B. C. *Electrochim. Acta* **2011**, *56*, 10443−10449.
(20) Jeon, I.; Yang, H.; Lee, S.; Heo, J.; Seo, D. H.; Shin, J.; Chung, U.; Kim, Z. G.; Chung, H.; Seo, S. *ACS Nano* **2011**, *5* (3), 1915−1920.
(21) Dickerson, J. H. *Electrophoretic Deposition of Nanomaterials*; Dickerson, J. H., Boccaccini, A. R., Eds.; Springer: New York, 2012; Chapter 3, p 132.
(22) Hasan, S. A.; Rigueur, J. L.; Harl, R. R.; Krejci, A. J.; Gonzalo-Juan, I.; Rogers, B. R.; Dickerson, J. H. *ACS Nano* **2010**, *4* (12), 7367−7372.
(23) Hu, W.; Peng, C.; Luo, W.; Lv, M.; Li, X.; Li, D.; Huang, Q.; Fan, C. *ACS Nano* **2010**, *4*, 4317−4323.
(24) Sundaram, R. S.; Gómez-Navarro, C.; Balasubramanian, K.; Burghard, M.; Kern, K. *Adv. Mater.* **2008**, *20*, 3050−3053.
(25) Hilder, M.; Winther-Jensen, B.; Li, D.; Forsyth, M.; MacFarlance, D. R. *Phys. Chem. Chem. Phys.* **2011**, *13*, 9187−9193.
(26) Moon, I. K.; Lee, J.; Ruoff, R. S.; Lee, H. *Nat. Commun.* **2010**, *1*, 73.
(27) Pei, S.; Cheng, H. *Carbon* **2012**, 3210−3228.
(28) Chen, C.; Huang, J.; Zhang, Q.; Gong, W.; Yang, Q.; Gong, M.; Yang, Q.; Wang, M.; Yang, Y. *Carbon* **2012**, *50*, 659−667.
(29) Zhang, H.; Zhang, X.; Zhang, D.; Sun, X.; Lin, H.; Wang, C.; Ma, Y. *J. Phys. Chem. B* **2013**, *117*, 1616−1627.
(30) Chavez-Valdez, A.; Shaffer, M. S. P.; Boccaccini, A. R. *J. Phys. Chem. B* **2013**, *117*, 1502−1515.
(31) Eda, G.; Fanchini, G.; Chhowalla, M. *Nat. Nanotechnol.* **2008**, *3*, 270−274.
(32) Wang, Y.; Zheng, Y.; Xu, X.; Dubuisson, E.; Bao, Q.; Lu, J.; Loh, K. P. *ACS Nano* **2011**, *5* (12), 9927−9933.
(33) Lee, V.; Whittaker, L.; Jaye, C.; Baroudi, K. M.; Fischer, D. A.; Banerjee, S. *Chem. Mater.* **2009**, *21*, 3905−3916.
(34) Xiao, F.; Song, J.; Gao, H.; Zan, X.; Xu, R.; Duan, H. *ACS Nano* **2012**, *6*, 100−110.
(35) Eda, G.; Chhowalla, M. *Adv. Mater.* **2010**, *22*, 2392−2415.
(36) Yang, D.; Velamakanni, A.; Bozoklu, G.; Park, S.; Stoller, M.; Piner, R. D.; Stankovich, S.; Jung, I.; Field, D. A.; Ventrice, C. A., Jr.; Ruoff, R. S. *Carbon* **2009**, *47*, 145−152.
(37) Jin, M.; Jeong, H.; Kim, T.; So, K. P.; Cui, Y.; Yu, W. J.; Ra, E. J.; Lee, Y. H. *J. Phys. D: Appl. Phys.* **2010**, *43*, No. 275402.
(38) Lu, T.; Pan, L.; Li, H.; Nie, C.; Zhu, M.; Sun, Z. *J. Electroanal. Chem.* **2011**, *661*, 270−273.
(39) Smits, F. M. *Bell Syst. Tech. J.* **1958**, 711−718.